






## Article

# Accelerated In Vitro Degradation of Optically Clear Low $\beta$ -Sheet Silk Films by Enzyme-Mediated Pretreatment

Ke Shang<sup>1</sup> , Jelena Rnjak-Kovacina<sup>1</sup> , Yinan Lin<sup>1</sup> , Rebecca S. Hayden<sup>1</sup> ,  
Hu Tao<sup>1</sup> , and David L. Kaplan<sup>1</sup> 

<sup>1</sup> Department of Biomedical Engineering, Tufts University, Medford, MA

**Correspondence:** David L. Kaplan, Department of Biomedical Engineering, Tufts University, 4 Colby Street, Medford, MA, USA. e-mail: david.kaplan@tufts.edu.

**Received:** 2 August 2012

**Accepted:** 5 February 2013

**Published:** 25 June 2013

**Keywords:** corneal tissue engineering; silk; films; degradation;  $\beta$ -sheet content; protease pretreatment

**Citation:** Shang K, Rnjak-Kovacina J, Lin Y, Hayden RS, Tao H, Kaplan DL. Accelerated in vitro degradation of optically clear low  $\beta$ -sheet silk films by enzyme-mediated pretreatment. *Trans Vis Sci Tech.* 2013;2(3):2. <http://tvstjournal.org/doi/full/10.1167/tvst.2.3.2>, doi:10.1167/tvst.2.3.2

**Purpose:** To design patterned, transparent silk films with fast degradation rates for the purpose of tissue engineering corneal stroma.

**Methods:**  $\beta$ -sheet (crystalline) content of silk films was decreased significantly by using a short water annealing time. Additionally, a protocol combining short water annealing time with enzymatic pretreatment of silk films with protease XIV was developed.

**Results:** Low  $\beta$ -sheet content (17%–18%) and enzymatic pretreatment provided film stability in aqueous environments and accelerated degradation of the silk films in the presence of human corneal fibroblasts in vitro. The results demonstrate a direct relationship between reduced  $\beta$ -sheet content and enzymatic pretreatment, and overall degradation rate of the protein films.

**Conclusions:** The novel protocol developed here provides new approaches to modulate the regeneration rate of silk biomaterials for corneal tissue regeneration needs.

**Translational Relevance:** Patterned silk protein films possess desirable characteristics for corneal tissue engineering, including optical transparency, biocompatibility, cell alignment, and tunable mechanical properties, but current fabrication protocols do not provide adequate degradation rates to match the regeneration properties of the human cornea. This novel processing protocol makes silk films more suitable for the construction of human corneal stroma tissue and a promising way to tune silk film degradation properties to match corneal tissue regeneration.

## Introduction

A transparent, avascular, elastic cornea protects the eye from the exterior environment, providing 75% of refractive power by forming a sharp image at the retinal receptors.<sup>1–3</sup> As the most commonly transplanted tissue in the United States, the supply of healthy corneas does not meet current clinical demand<sup>2,4–5</sup> and, therefore, successful tissue engineering of human cornea would address a major need. Tissue engineered epithelium and endothelium have been effectively studied and tested in animal models; however, the cornea stroma, which accounts for 90% of corneal thickness, remains challenging to reconstruct due to its complex structural hierarchy.<sup>6</sup>

Human central corneal stroma consists of stacked collagen fibril lamellae populated by quiescent keratocyte cells. In each lamella, type I and type V collagen

fiber bundles run parallel to each other with regular interfibrillar spacing. Collagen fibrils in the stroma show preferred alignment in horizontal and vertical directions<sup>3,7–9</sup> arranged in a pseudo crystalline lattice orientation.<sup>2,10</sup> The specific collagen orientation contributes to the mechanical strength and the optical clarity of the cornea.<sup>3,11</sup> The special arrangement of the parallel lamellae with spacing less than one light wavelength and the uniform spacing of the fibers cause “destructive interference” of incoming light rays. The destructive interference reduces light scatter and leads to corneal transparency.<sup>3,11</sup> Isotropically organized collagen fibrils balance intraocular pressure while fibrils aligned along the superior–inferior and nasal–temporal meridians withstand the tensile stress from the orbicularis and rectus muscles.<sup>12</sup>

Recent interest in corneal tissue engineering has prompted the development of a range of biomaterials with specific features aimed at mimicking the complex

stromal structure and function. However, due to the complexity of the structural hierarchy and requirements for mechanical strength and optical transparency, the development of a corneal equivalent remains challenging. Silk fibroin is a promising biomaterial for a range of tissue engineering and regenerative medicine purposes due to its abundance, biocompatibility, mechanical robustness, and tunable degradation properties. Silk also possesses a unique set of features that make it a promising candidate for successful corneal tissue engineering. Silk can be cast into thin (3–4  $\mu\text{m}$ ), optically transparent films with surface features that have been optimized for corneal fibroblast alignment.<sup>6</sup> Over 14 days in culture on these films, corneal fibroblasts express important markers of corneal stroma, including collagen V, decorin, and biglycans. These extracellular matrix (ECM) components, as well as the cellular cytoskeletal filaments were oriented along the aligned, patterned grooves in silk films.<sup>6</sup> The advantage of this system over many other technologies developed as corneal stroma equivalents is that the complex multilamellar arrangement of the stromal cells and their associated ECM can be recapitulated. By stacking multiple silk films (seeded with corneal fibroblasts) in helicoidal, multilamellar arrangement, a single, cellular, optically transparent stromal equivalent can be generated.<sup>7,13</sup> Furthermore, the relative ease of silk surface modification allows silk films functionalization with the arginine-glycine-aspartic acid (RGD) cell adhesion peptide, thereby, significantly improving corneal fibroblast attachment and proliferation on silk matrices.<sup>7</sup>

In order for these constructs to serve as clinically-relevant corneal equivalents, their degradation rate needs to match the rate of corneal regeneration. Silk degradation correlates with its  $\beta$ -sheet structure, consisting of highly repetitive alanine-glycine or alanine repeats. Increased ratio of  $\beta$ -sheet structure in silk leads to lower rates of enzymatic degradation by protease XIV and  $\alpha$ -chymotrypsin.<sup>14</sup> The  $\beta$ -sheet structure determines the stabilization of silk in aqueous environments.<sup>15</sup> For this reason, the  $\beta$ -sheet structure needs to be induced into regenerated silk to ensure water resistance of silk films.<sup>15</sup> The  $\beta$ -sheet-inducing process includes treatment with methanol, ethanol, or physical methods such as water vapor annealing and slow drying<sup>16–18</sup> to generate the physical crosslinks in the crystals. Among the above methods, water vapor annealing is the most controllable.<sup>18</sup> The current water annealing protocol for silk films used in corneal tissue engineering (2 hour water annealing at 25°C) generates

films that do not degrade after 3 months when implanted in rabbit corneal pockets (unpublished data) and, therefore, warrants further investigation toward more rapidly degrading films that maintain structural integrity, allow surface patterning, and remain optically transparent. Reduced  $\beta$ -sheet content will result in a less compacted structure for easier access by proteolytic enzymes and, thus, faster hydrolysis, making it possible to adjust the degradation properties to match tissue regeneration and ensure optimum mechanical and physiologic integration.<sup>17</sup>

In the present study, short water annealing (low  $\beta$ -sheet content) times and an enzymatic pretreatment were combined to increase the degradation rate of silk films for corneal tissue engineering. Silk film degradation by bacterial protease XIV and human pancreatic  $\alpha$ -chymotrypsin was used to confirm the  $\beta$ -sheet content related to degradation rate. Human corneal fibroblasts (hCFs) produce metalloproteinases capable of degrading basement membrane components.<sup>19</sup> Among matrix metalloproteinases (MMPs) produced by human corneal cells, MMP-1, MMP-2, MMP-3, and MMP-4 have recognition sites that are present in silk fibroin.<sup>20,21</sup> Therefore, hCFs were utilized in vitro to biologically assess the degradation of these silk films with different  $\beta$ -sheet contents and with enzyme pretreatment.

## Methods

### Preparation of Regenerated Silk Fibroin Solutions

All procedures followed our prior published methods.<sup>22</sup> *Bombyx mori* silk cocoons from Tajima Shoji Co., LTD (Sumiyoshicho, Naka-ku, Yokohama, Japan) were cut into fourths. For every 5 g of cocoon degumming proceeded for 20 minutes in boiling 0.02 M sodium carbonate solution to remove the glue-like sericin proteins from the silk fibroin proteins. The fibroin fiber extract was rinsed 6 to 7 times in distilled water and air dried overnight. The dried degummed silk fibers were dissolved in 9.3 M lithium bromide solution at a ratio of 1 g of silk fibers per 4 mL of LiBr solution in 60°C oven for 4 hours. The solution was placed in a cellulose membrane based Slide-A-Lyzer dialysis cassette (MWCO3500; Pierce Biotechnology, Rockford, IL) and dialyzed against distilled water for 48 hours to remove lithium bromide salt. The dialyzed silk solution was then centrifuged twice at 8800 rpm for 20 minutes. The supernatant was collected and stored at 4°C. The final concentration of aqueous silk solution

was between 5 and 7 wt/vol percent, determined by gravimetric analysis.<sup>13</sup>

### Preparation of Polydimethylsiloxane (PDMS) Molds for Silk Casting

Patterned PDMS (Sylgard 184 Silicone Elastomer Kit; Dow Corning, Midland, MI) substrates of 1.5- to 3.0-mm thickness were generated by casting on a patterned optical mirror surface with grooves of 3.5- $\mu\text{m}$  width and 500-nm depth (Edmund Optics, Inc, Barrington, NJ). The PDMS substrates were placed cast side up and prepared for silk solution casting.<sup>13,23</sup>

### Preparation of Silk Films from Regenerated Silk Fibroin Solutions

A 1.1 mL aliquot of 1 wt/vol percent silk solution was cast upon grooved PDMS molds resulting in 3- to 4- $\mu\text{m}$  thick films after drying. The films were covered with a venting lid and allowed to dry overnight in a chemical hood. Once dry, the films were water annealed in a vacuum oven with a 200 mL water tray at the bottom at 25°C, 20 mm Hg vacuum for 30 to 60 minutes to obtain silk films with different levels of  $\beta$ -sheet. After annealing and drying, the silk film margins were sealed with Scotch Tape (Hutchinson, MN) to form a frame to prevent the films from collapsing when wet.

### Fourier Transform Infrared Spectroscopy Analysis

To assess the secondary structure of the silk films, Fourier transform infrared spectroscopy (FTIR) analysis was performed by a multiple reflection, horizontal MIRacle attenuated total reflectance (ATR) (Ge crystal; Pike Tech., Madison, WI) attached Jasco FT/IR-6200 spectrometer (JASCO, Tokyo, Japan), using our previously published procedures.<sup>18</sup> For each mid-infrared spectrum (400 ~ 4000  $\text{cm}^{-1}$ ), 128 scans were collected in reflection mode at 4  $\text{cm}^{-1}$  resolution. The Amide I bands (1595 ~ 1705  $\text{cm}^{-1}$ ) were resolved by Fourier self-deconvolution (FSD) in the Opus 5.0 software package (Bruker Optics, Billerica, MA) using a Lorentzian line shape and parameters equivalent to 20  $\text{cm}^{-1}$  bandwidth at half height and a noise suppression factor of 0.3. Gaussian curve-fitting was conducted on the amide I spectra after resolution enhancement FSD. The  $\beta$ -sheet content of silk films was calculated from the areas of the individual assigned bands and their fraction of the total area in the amide I region. The peak absorption bands at 1610 to 1625 and 1696 to 1704  $\text{cm}^{-1}$  were assigned as  $\beta$ -sheet

structure; the peak from 1640 to 1650  $\text{cm}^{-1}$  was random coil structure; 1650 to 1660  $\text{cm}^{-1}$  was alpha-helical bands position; and 1660 to approximately 1695  $\text{cm}^{-1}$  was peak position for  $\beta$  turns. For each type of silk film, the conformational characterization was carried out on at least three samples prepared independently. Further comparison among the three types of silk films was made based on the average percentage of secondary structure.<sup>18</sup>

### Preparation and Screening of Silk Films with Different $\beta$ -Sheet Contents

To prepare silk films with different  $\beta$ -sheet content, water annealing, and methanol treatment were used. Low  $\beta$ -sheet content silk film was generated by room temperature water vapor annealing for 30 to 45 minutes. Silk films with this  $\beta$ -sheet level were just water stable with a  $\beta$ -sheet content of 17% to 18%. Medium  $\beta$ -sheet content silk films were prepared by room temperature water vapor annealing for 45 to 60 minutes ( $\beta$ -sheet content 23%–24%). High  $\beta$ -sheet silk films were produced by treating the films with methanol for 5 minutes to achieve around 55%  $\beta$ -sheet content. High  $\beta$ -sheet content films for cell culture studies were achieved by water vapor annealing using boiling water for 15 minutes, generating 43% to 45%  $\beta$ -sheet content.

### Transmission Measurements

Transmission spectra of silk films with different beta sheet contents were measured by placing the samples in close proximity between two optical fiber probes (distance ~5 mm) that couple to a portable spectrometer (time constant: 5 ms; average number: 10; wavelength: 350 nm–1000 nm, USB2000; Ocean Optics, Dunedin, FL).

### Enzymatic Pretreatment

Some of low  $\beta$ -sheet silk films were pretreated with 0.0125 U/mL protease XIV for 24 hours to further accelerate silk film degradation.

### RGD Surface Modification

RGD functionalization followed our previously published procedures.<sup>24</sup> The silk films were pre-soaked in BupH MES buffered saline, pH 6.0 (Thermo Scientific, Waltham, MA) solution for 30 minutes. The -COOH groups from the silk fibroin were activated with 1-ethyl-3-(dimethylaminopropyl) carbodiimide hydrochloride (EDC-HCl)/N-hy-

droxysuccinimide (NHS) solution for 30 minutes at room temperature, generating amine-reactive NHS-esters on the silk film surface. The films were washed with 2-(*N*-morpholino)ethanesulfonic acid (MES) buffer three times and subsequently treated in 1 mg/mL glycine-arginine-glycine-aspartic acid-serine (GRGDS) peptide (Bachem, Torrance, CA) in MES buffer, pH 6.0 at room temperature for 2 hours.<sup>5</sup> After the GRGDS coupling reaction, the surface modified silk films were washed twice in MES buffer and five times in double distilled water. Silk films were sterilized by ultraviolet (UV) light in biosafety hoods on both sides of silk film overnight.

### Enzyme Degradation

Silk film samples of 15 mg ( $\pm 1$  mg) with low, medium, and high  $\beta$ -sheet content were incubated at 37°C in phosphate-buffered saline (PBS) solution containing protease XIV from *Streptomyces griseus* (EC 3.4.24.31) or  $\alpha$ -chymotrypsin from human pancreas (EC3.4.21.1) in 1.5 mL Eppendorf tubes (Eppendorf, Hauppauge, NY). Serial enzyme concentrations were applied to identify the degradation differences of silk films with different amounts of  $\beta$ -sheet. Degradation studies were performed with 0.1, 0.05, and 0.025 U/mL Protease XIV and 1, 0.5, and 0.25 U/mL  $\alpha$ -chymotrypsin in PBS.<sup>25</sup> At daily time points, silk film residues were centrifuged at 10,000 rpm for 10 minutes and wash twice with Milli-Q water (Life Technologies, Grand Island, NY). After rinsing, silk films residues were centrifuged again at 10,000 rpm for 10 minutes to collect the silk residues. The silk film residues were dried overnight in a chemical hood and the mass determined using an analytical balance. Fresh enzyme solution was added to each tube and the samples were incubated at 37°C. Six samples from each group were taken at each time point to get statistically significant data ( $N = 6$ ). Samples incubated in PBS at 37°C without enzymes served as controls.<sup>18</sup>

### Human Corneal Fibroblast Cell Culture and Silk Film Seeding

Primary hCFs isolated from donor corneas (provided by May Griffith, University of Ottawa Eye Institute) were cultured in Dulbecco's Modified Eagle Medium (DMEM; Life Technologies, Grand Island, NY) with high glucose and GlutaMAX (Invitrogen, Grand Island, NY) containing 10% fetal bovine serum (FBS) and 1% antibiotic-antimycotic (Invitrogen).

Cells were maintained at 37°C in a 5% CO<sub>2</sub> incubator. The cultures were detached from their substrates using 0.25% Trypsin (Invitrogen). The hCF cells were seeded on sterile square silk films (1.5 × 1.5 cm<sup>2</sup>) with varying  $\beta$ -sheet contents at a cell density of 20,000 cells/cm<sup>2</sup> for 8 weeks.<sup>5</sup> Nonseeded silk films with different  $\beta$ -sheet contents served as controls. Cell proliferation rates on silk films were analyzed by Alamar blue (Life Technologies, Grand Island, NY) at day 1, 7, and 14 according to manufacturer's protocol. Cell number at each time point was normalized to seeding number at day 0. Silk film degradation by hCFs was examined by scanning electron microscopy (SEM) at week 2, 4, 6, and 8 post seeding following cell detachment as described below.

### Scanning Electron Microscopy

Morphological analysis of degraded silk films was performed by SEM (Zeiss UltraPlus SEM or Zeiss Supra 55 VP SEM; Carl Zeiss SMT Inc., Peabody, MA) at a voltage of 2 to 3 kV. During hCF cell degradation, samples were taken at 2 weeks intervals until week 8. After trypsinizing the hCF cells, the silk films were punched into round biopsies of 10-mm diameter. Silk film biopsies were progressively dehydrated twice in a graded series of ethanols (50%, 70%, 80%, 90%, 95%, and in 100%, 10 minutes at each concentration). The samples were subsequently dried by hexamethyldisilazane (HMDS; Electron Microscopy Science, Hatfield, PA) overnight. After drying samples were coated with a thin (10 nm) layer of platinum/palladium using a sputter coater (208HR; Cressington Scientific Instruments Inc., Cranberry Twp, PA) prior to imaging. The roughness increase of degraded silk films was quantified by MeX software (Alicona, Bartlett, IL) on three samples. Average Roughness (Ra) was calculated based on the formula:  $Ra = 1/n \sum_{i=1}^n |y_i|$ . Root mean square roughness (Rq) was calculated based on the formula:  $Rq = \sqrt{\frac{1}{n} \sum_{i=1}^n y_i^2}$ . To compare the dimensions of the degradation features, the length, width, and area of 10 irregular degradation pits was measured ( $N = 10$ ) using ImageJ image processing and analysis software (National Institutes of Health, Bethesda, MD) across diametrically opposite ends of the pits. The pit distribution density was counted based on seven views. The numbers of degradation holes and cracks were determined based on measurements from three views.

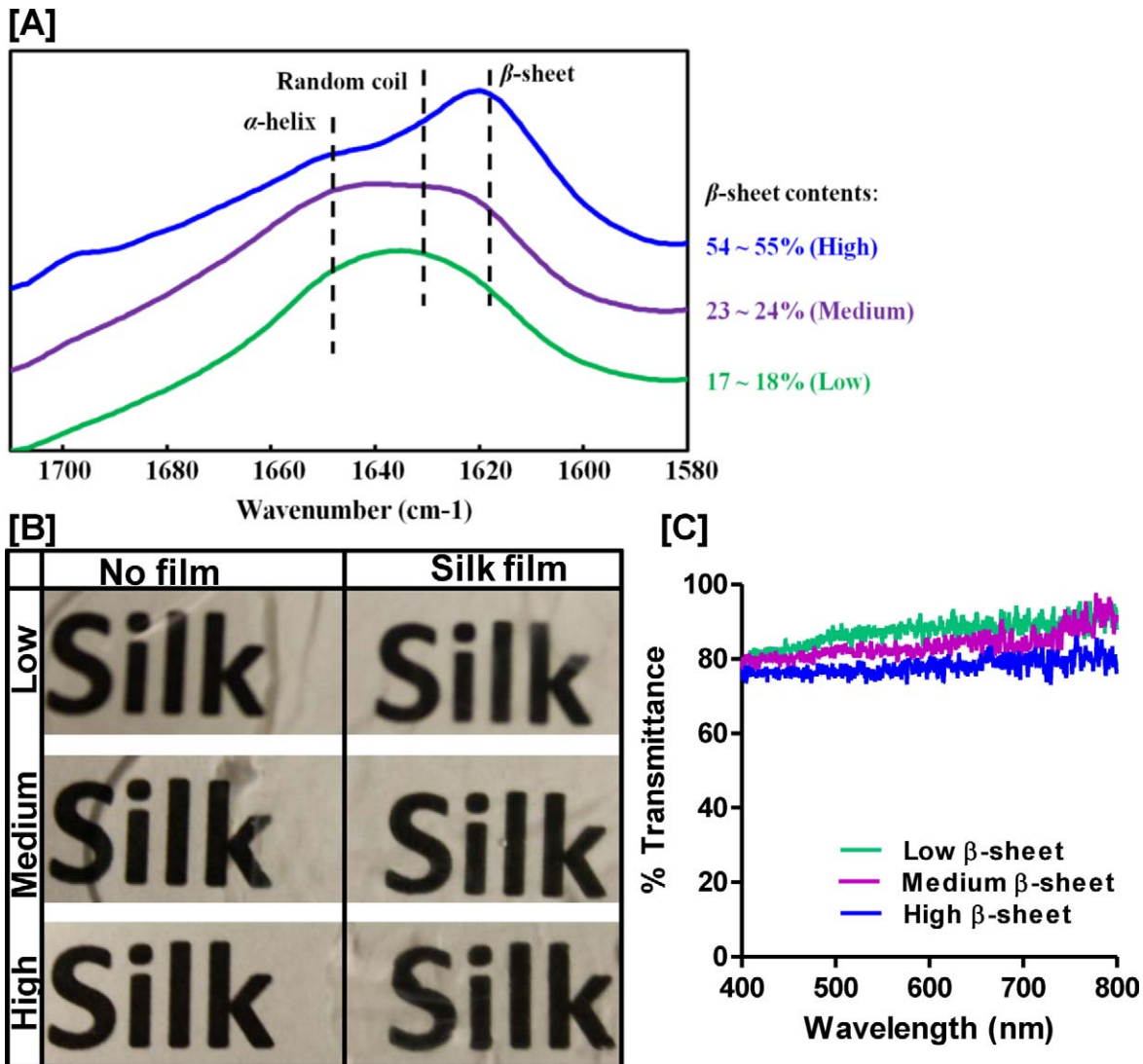


**Figure 1.** (A) FTIR spectra of the Amide I region of the silk films with various  $\beta$ -sheet contents: low (bottom), medium (middle) and high (top). The percentages of  $\beta$ -sheets were determined by Fourier self-deconvolution. (B) Photographs of hydrated silk films with different  $\beta$ -sheet contents (low, medium, high) placed over a piece of paper displaying the word 'silk'. (C) Transmittance measurements of silk films with different  $\beta$ -sheet contents (low, medium, high) in the visible light range.

## Statistical Analyses

All data are presented as mean  $\pm$  SD. Statistical analyses were performed by using one-way or two-way analysis of variance (ANOVA) to calculate differences.  $P$  less than 0.05 were regarded as statistically significant. Statistically significant differences are indicated as \* ( $P < 0.05$ ), \*\* ( $P < 0.01$ ), and \*\*\* ( $P < 0.001$ ).

## Results

### Water Resistant Silk Films Produced by

### Water Vapor Annealing-Induced Physical $\beta$ -Sheet Cross-Links

Silk films with various  $\beta$ -sheet contents were produced by water vapor annealing or methanol immersion and were studied by FTIR spectroscopy. Deconvolution of the amide I region was performed for secondary structure quantification. Methanol immersed silk films (top curve in Fig. 1A) showed a strong absorption peak centered at 1610 to 1625  $\text{cm}^{-1}$ , which was assigned to the  $\beta$ -sheets of silk.<sup>18</sup> These films had 54% to 55%  $\beta$ -sheet content and were classified as 'high  $\beta$ -sheet films'. Silk films water vapor annealed for 30 to 45 minutes had  $\beta$ -sheet

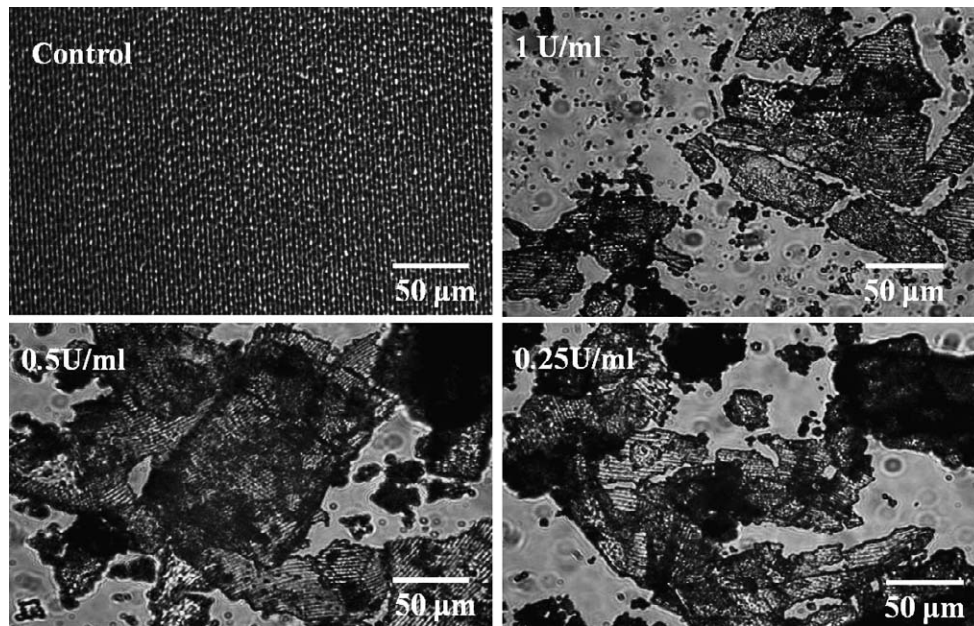


**Figure 2.** Optical micrographs of bulk degraded silk films in  $\alpha$ -chymotrypsin at various concentrations after 4 days of degradation.

content of 17% to 18% and were deemed ‘low  $\beta$ -sheet films’ as shorter treatments resulted in films with no structural integrity that dissolved in aqueous environments. The secondary structure of ‘low  $\beta$ -sheet films’ (bottom curve in Fig. 1A), was dominated by random coil conformations ( $1640\text{--}1650\text{ cm}^{-1}$ ). ‘Medium  $\beta$ -sheet films’ were produced by water vapor annealing at  $25^\circ\text{C}$  for 45 to 60 minutes and showed increased  $\beta$ -sheet content compared with the low  $\beta$ -sheet silk films as demonstrated by the small shoulder peak (middle curve in Fig. 1A) and  $\beta$ -sheet content of 23% to 24%. Low, medium and high  $\beta$ -sheet films were structurally stable, possessed clear grooved patterns necessary for cell alignment and were optically transparent (Fig. 1B, 1C).

### Degradation of Silk Film in Vitro by Human Pancreatic $\alpha$ -Chymotrypsin

The  $\alpha$ -chymotrypsin from human pancreas was used to degrade silk films at concentrations of 1, 0.5, and 0.25 U/ml. No degradation occurred on the control silk films incubated in PBS without enzyme. Bulk degradation was observed in the optical micrographs of all the silk films incubated with  $\alpha$ -chymotrypsin at day 4 (Fig. 2). The films broke into pieces with the nanometer scale film pattern remaining mostly intact. The remaining mass of silk films over time was quantified by weighing the silk film residues after drying (Fig. 3A). Silk degradation level

correlated with  $\beta$ -sheet content, where high  $\beta$ -sheet films showed no significant mass loss over 4 days with  $\alpha$ -chymotrypsin concentrations up to 1 U/mL, while low  $\beta$ -sheet showed significantly more mass loss compared with medium  $\beta$ -sheet films at all enzyme concentrations (Fig. 3A).

### Degradation of Silk Films In Vitro by Protease

Unlike  $\alpha$ -chymotrypsin, high  $\beta$ -sheet films showed 3% and 12% mass loss at 0.05 U/mL and 0.1 U/mL of enzyme. Mass differences between low and medium, as well as low and high  $\beta$ -sheet films were significant at day 4 at all enzyme concentrations.

### Human Corneal Fibroblast Cells Proliferation on Silk Films with Various $\beta$ -Sheet Levels

hCFs were seeded on silk films with different  $\beta$ -sheet contents (low, medium, and high) to assess the effect of  $\beta$ -sheet content on cell proliferation and therefore ensure that film degradation in the presence of cells correlates with  $\beta$ -sheet content and is not affected by differences in cell number on different treatments. No significant difference was observed in cell numbers on different silk films over a 15 day period, assessed by Alamar blue metabolic assay (Fig. 4). At week 2 post seeding, the cells were aligned and completely confluent on all the films.

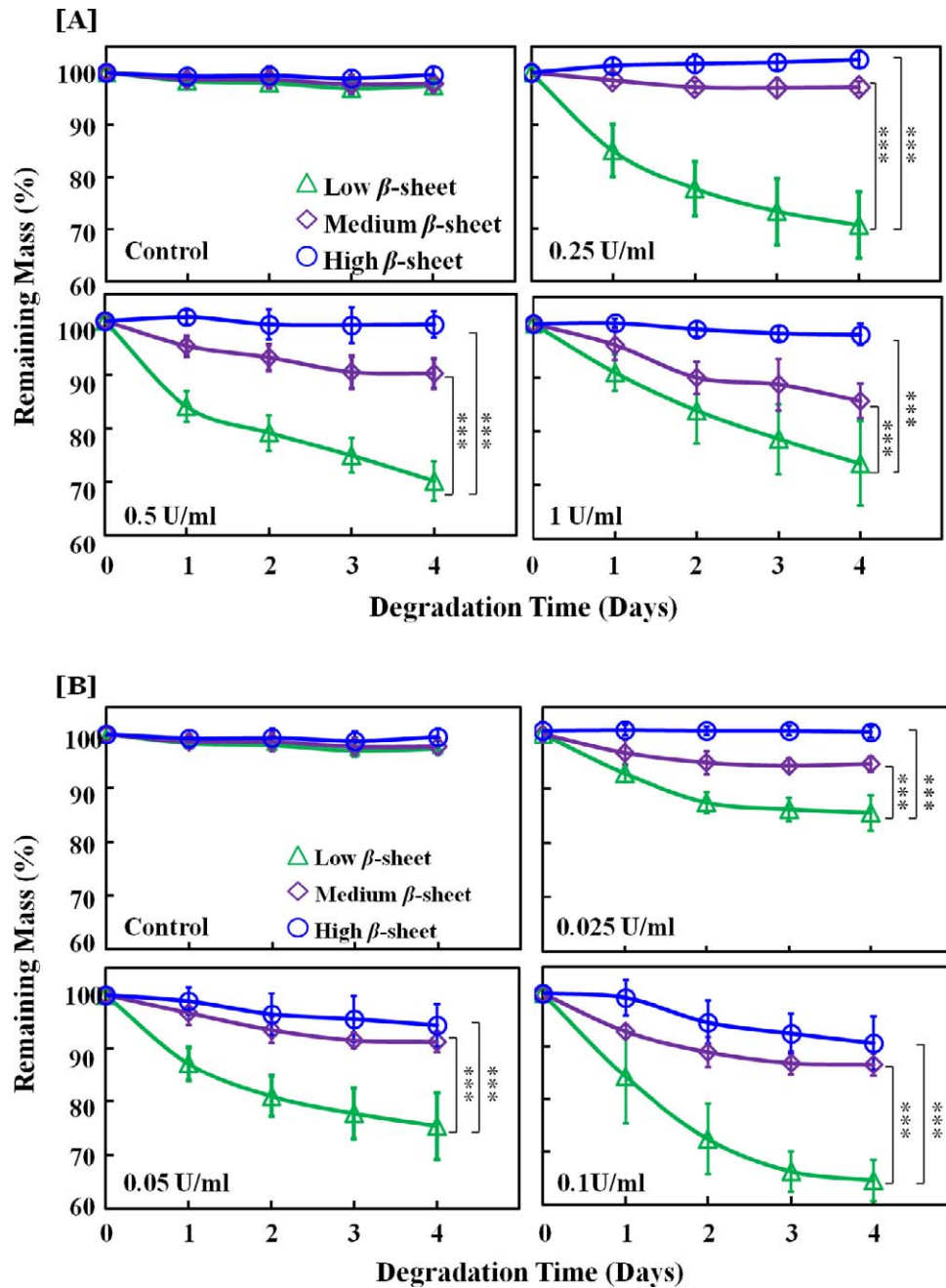


**Figure 3.** Time-dependent enzyme degradation profiles of silk films with various  $\beta$ -sheet contents with (A) human pancreatic  $\alpha$ -chymotrypsin and (B) bacterial protease XIV. Film degradation is expressed as percent remaining mass, such that lower remaining mass indicates greater level of film degradation.

### Cell Degradation of Silk Films with Different $\beta$ -Sheet Levels

Since there was no proliferation difference among hCFs on silk films with different  $\beta$ -sheet content, hCFs were seeded on the different films at the same density and cultivated to compare degradation differences of silk films. In order to assist cell

degradation in addition to the lower  $\beta$ -sheet content films, protease XIV enzyme pretreated films were also assessed. Silk film degradation by hCFs was assessed by analyzing surface roughness and quantifying degradation features on the film surface following cell removal from the silk films at 2, 4, 6, and 8 weeks post seeding. In order to quantify the process at the early stages when no obvious degradation features

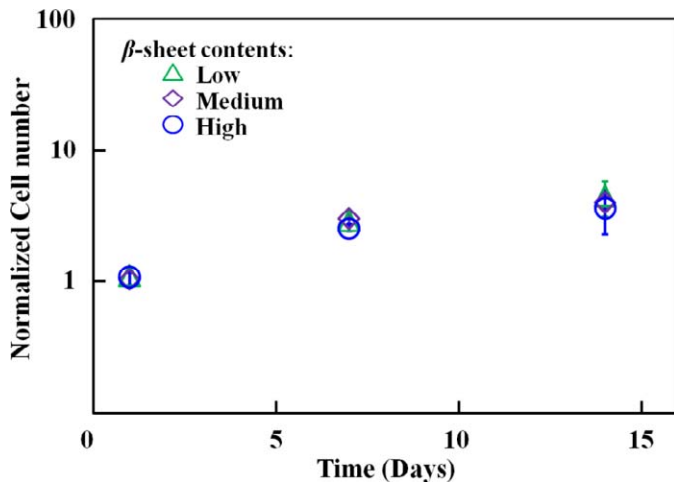


**Figure 4.** Equivalent hCF cell proliferation behavior on silk films with various  $\beta$ -sheet levels. The cell number was normalized to initial cell number seeded on each silk film.

were observed, roughness changes on the film surfaces were monitored. The most commonly assessed roughness parameter, average roughness (Ra) and root mean square roughness (Rq), a parameter that measures the variance of the amplitude distribution function were monitored on low, medium, and high  $\beta$ -sheet films and on enzyme pretreated films following incubation with hCFs (Fig. 5). Enzyme pretreatment caused a 23% increase in the film surface roughness (Ra and Rq) prior to incubation with hCFs, but did not affect the structural integrity or optical transparency of the silk films. Films pretreated with enzyme also showed the greatest overall increase in Ra and Rq in the presence of hCFs, with Ra increasing 1.6-fold and Rq increasing 1.4-fold by week 8 post seeding. At week 8 post seeding, Ra and Rq of enzyme pretreated silk films were significantly higher

compared with all nontreated films. The Ra of low  $\beta$ -sheet films increased 1.3-fold by week 8 post seeding, compared with 0.2-fold increase in medium and 0-fold increase in high  $\beta$ -sheet films (Fig. 5A). Similarly, Rq of low  $\beta$ -sheet films increased by 1.2-fold, compared with 0.3-fold and 0-fold increase in medium and high  $\beta$ -sheet films, respectively.

By week 8 post seeding, hCF cells formed degradation features on the enzyme pretreated films, but not on the other films. The degradation features included degradation pits, cracks, and holes (Fig. 6). Degradation pits were shallow pits where surface pattern grooves of silk films were eroded due to hCF degradation (Fig. 6B). Small degradation holes formed along the base of the grooves in the patterned silk films and a number of small degradation holes connected together to form degradation cracks. Unlike the degradation pits which crossed the grooves, the degradation cracks formed along the grooves of the patterned silk films, where the films were eroded and split (Fig. 6C). The dimensions and numbers of the above degradation features were quantified (Tables 1, 2). Degradation pits for enzyme pretreated low  $\beta$ -sheet silk films presented at  $150 \pm 80 /\text{mm}^2$ , were around  $3 \pm 0.8 \mu\text{m}$  in length,  $2 \pm 1 \mu\text{m}$  in width and  $10 \pm 7 \mu\text{m}^2$  in area. There were around 300 smaller degradation holes and 36 cracks formed per millimeter groove. Since smaller holes linked together to form cracks, the ratio of small holes and cracks was also counted at 10:1.

## Discussion

Patterned silk films are promising biomaterial candidates for engineering the complex hierarchical structure of the human cornea, but do not degrade

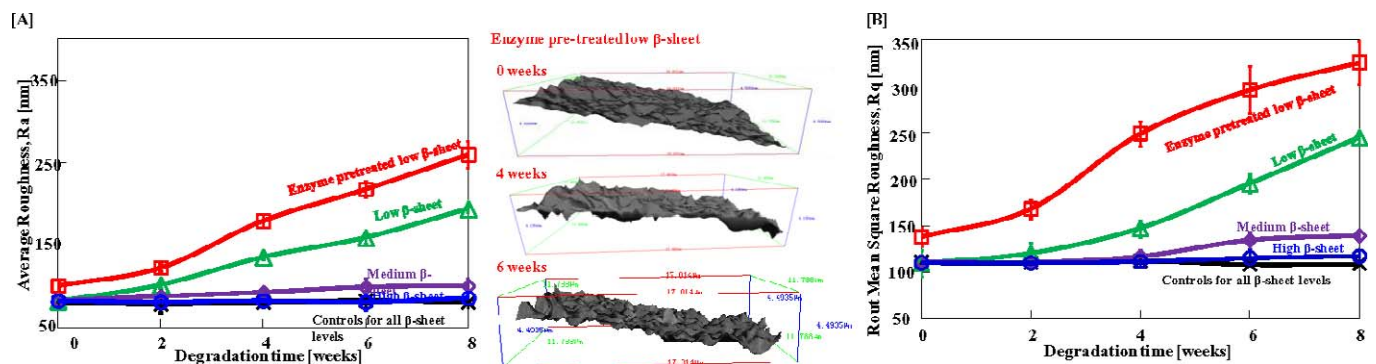


**Figure 5.** Increase in surface roughness features induced by hCF degradation over an 8 week culture period quantified from SEM images of decellularized samples using MeX software. (A) Ra quantification (left) and three-dimensional reconstruction of the control surfaces (0 weeks) and following 4 and 6 weeks of cell culture. (B) Rq quantification.



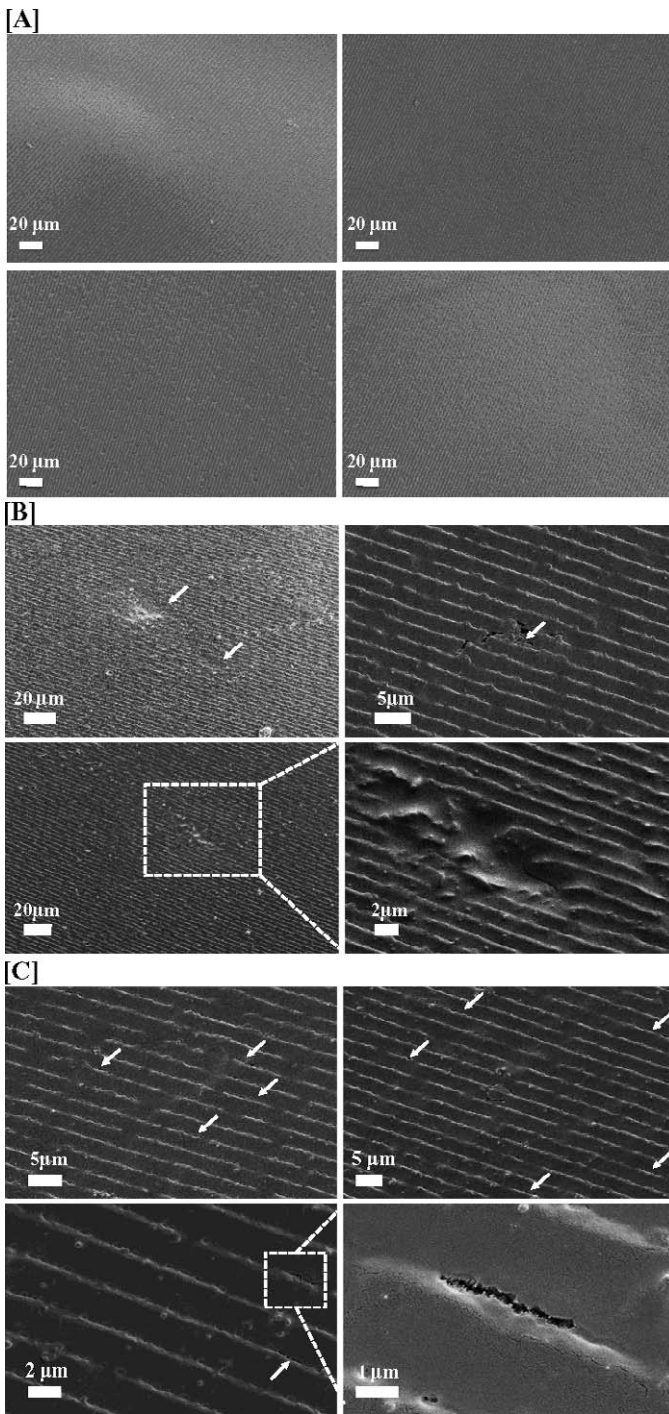


**Figure 6.** Scanning electron micrographs of the silk films after degradation with hCF for 8 weeks. (A) Control samples incubated in media with no cells, (B, C) samples incubated with hCF showing (B) degradation pits (arrows) and (C) degradation holes and cracks (arrows). One of the cracks was zoomed in the right bottom corner.

**Table 1.** Degradation Pit Dimensions (Mean  $\pm$  SD)

Density ( $\text{mm}^2$ )	150 ( $\pm 80$ )
Length ( $\mu\text{m}$ )	3 ( $\pm 0.8$ )
Width ( $\mu\text{m}$ )	2 ( $\pm 1$ )
Area ( $\mu\text{m}^2$ )	10 ( $\pm 7$ )

fast enough to match corneal regeneration needs (no observable degradation after 3 months in a rabbit corneal pocket model, unpublished data). In this study, the degradation behavior of silk films with low  $\beta$ -sheet (17%–18%) content was compared with that of medium (23%–24%) and high (54%–55%)  $\beta$ -sheet content films. The level of crystallinity ( $\beta$ -sheet content) is strongly correlated to the degradation properties of silk materials.<sup>17,18</sup> Low  $\beta$ -sheet content contributes to a less-compacted/less crystalline structure that allows easier access by proteolytic enzymes and thus faster silk enzymatic hydrolysis.<sup>17</sup> However, some level of crystallinity is necessary to stabilize the silk structure in aqueous environments.<sup>26</sup> Therefore, a trade off exists between fast degradation and stability of silk films in aqueous environments. A minimum  $\beta$ -sheet content of 17%–18% was necessary to maintain structural stability and integrity of patterned, optically transparent silk films. Lowered  $\beta$ -sheet content did not adversely affect the optical properties of silk films, in fact, silk films with low and medium  $\beta$ -sheet content showed a slight improvement in light transmittance properties in the visible range. The effect of  $\beta$ -sheet content on the mechanical properties of silk films has been previously described. Silk films with low and medium  $\beta$ -sheet content described here are expected to display a modulus of elasticity between 10 and 30 MPa, yield stress between 1.5 and 2 MPa and tensile strength between 2 and 2.5 MPa.<sup>18</sup> These low  $\beta$ -sheet films displayed faster enzymatic degradation rates compared with medium and high  $\beta$ -sheet films in the presence of  $\alpha$ -chymotrypsin and protease XIV. Previous research demonstrated that protease XIV from *S. griseus* caused the most significant degradation of silk materials, degrading both amorphous, and crystalline regions.<sup>14,27</sup> Unlike protease XIV,  $\alpha$ -chymotrypsin only degrades

**Table 2.** Degradation Hole and Crack Dimensions (Mean  $\pm$  SD)

Numbers of Holes/(mm groove)	300 ( $\pm 145$ )
Numbers of Cracks/(mm groove)	30 ( $\pm 14$ )
Holes/Cracks	10:1

the less crystalline domains in the silk<sup>28</sup> without activity toward the  $\beta$ -sheet crystals.<sup>14</sup> While neither of these enzymes are expressed in the human cornea, they are invaluable tools in studying the effects of material properties on silk construct degradation profiles in vitro. Both enzymes have been used extensively to study silk degradation, allowing new findings to be easily correlated with previously published findings. Degradation of silk materials has been demonstrated in numerous animal models,<sup>17</sup> as well with collagenases, enzymes known to be expressed in injured corneal tissue.<sup>25</sup>

The surface roughness properties (Ra and Rq) of low  $\beta$ -sheet silk films also increased to a greater extent compared with medium and high  $\beta$ -sheet films in the presence of hCFs in vitro. hCFs produce MMP-1, MMP-2, MMP-3, and MMP-9, which have recognition sites on silk fibroin.<sup>19,21,29,30</sup> However, other than an increase in surface roughness, hCFs did not generate other discernible degradation features on the silk films over the 8 week culture period. Other cell types, including osteoblasts, osteoclasts, and human mesenchymal stem cells have previously been shown to generate degradation features, including large 3- $\mu$ m pits on the patterned silk surfaces.<sup>31</sup>

To further enhance the degradation behavior of low  $\beta$ -sheet films, the films were pretreated with a low concentration (0.0125 U/mL) of protease XIV prior to cell culture. This treatment initiated the degradation of silk films without compromising the structural integrity. It is likely that protease XIV loosened the compact secondary structure of low  $\beta$ -sheet silk films, leading to the increased initial surface roughness and faster degradation. Enzyme pretreated films displayed the greatest increase in surface roughness (Ra and Rq) and higher overall surface roughness at 8 weeks post seeding. These films were also the only condition that displayed discernible degradation features on the film surface, including degradation pits, holes, and cracks. Most degradation features, especially degradation holes and cracks were observed along the base of the patterned grooves on the film surface. The width and the depth of these grooves were nanotopography parameters to align the cells.<sup>32</sup> As hCF cells aligned along the grooves, the edges of grooves were likely initially exposed to MMPs secreted by aligned cells, resulting in the degradation features observed. First, small degradation holes appeared along the grooves and this feature increased as the degradation holes connected into degradation cracks.

This study provided a protocol to significantly accelerate degradation of silk films starting with short

time water vapor annealing to generate low  $\beta$ -sheet (17%–18%) films, followed by enzymatic pretreatment with protease XIV. Lowering  $\beta$ -sheet content to the limit of water stability balanced the tradeoff between silk film structural integrity in aqueous environments and faster degradation rates, while enzyme pretreatment further enhanced degradation properties allowing initiation of film degradation by hCFs within an 8 week period. This novel processing protocol makes silk films more suitable for the construction of human corneal stroma tissue and a promising way to tune silk film degradation properties to match corneal tissue regeneration. Successful film degradation by hCFs in vitro warrants further investigation of these films in vivo. This protocol is also of potential utility in a broader range of biomaterial needs where more rapid degradation or remodeling rates would be advantageous in tissue repairs and regenerative medicine needs.

## Acknowledgments

The authors thank Xiao Hu for his help during the initial exploration of the  $\beta$ -sheet structure and water vapor annealing method, and also Biman B. Mandal for his contribution to the corneal tissue engineering project and his help during the early stages of this project.

This work was supported by the National Institutes of Health (NIH; EY020856) and the NIH P41 Tissue Engineering Resource Center (EB002520). This work was performed in part at the Center for Nanoscale Systems (CNS), a member of the National Nanotechnology Infrastructure Network (NNIN). CNS is part of the Faculty of Arts and Sciences at Harvard University.

Disclosure: **K. Shang**, None; **J. Rnjak-Kovacina**, None; **Y. Lin**, None; **R.S. Hayden**, None; **H. Tao**, None; **D.L. Kaplan**, None

## References

1. Sugioka K, Yoshida K, Kodama A, et al. Connective tissue growth factor cooperates with fibronectin in enhancing attachment and migration of corneal epithelial cells. *Tohoku J Exp Med.* 2010;222:45–50.
2. Shah A, Brugnano J, Sun S, Vase A, Orwin E. The development of a tissue-engineered cornea:

- biomaterials and culture methods. *Pediatr Res*. 2008;63:535–544.
3. West-Mays JA, Dwivedi DJ. The keratocyte: corneal stromal cell with variable repair phenotypes. *Int J Biochem Cell Biol*. 2006;38:1625–1631.
  4. Crabb RAB, Chau EP, Evans MC, Barogas VH, Hubel A. Biomechanical and microstructural characteristics of a collagen film-based corneal stroma equivalent. *Tissue Eng*. 2006;12:1565–1575.
  5. Gil ES, Mandal BB, Park SH, Marchant J, Omenetto FG, Kaplan DL. Helicoidal multilamellar features of RGD-functionalized silk biomaterials. *Biomaterials*. 2010b;31:8953–8963.
  6. Gil ES, Park SH, Marchant J, Omenetto FG, Kaplan DL. Response of human corneal fibroblast on silk film surface patterns. *Macromol Biosci*. 2010a;10:664–673.
  7. Abahussin M, Hayes S, Cartwright NEK, et al. 3D collagen orientation study of the human cornea using x-ray diffraction and femtosecond laser technology. *Invest Ophthalmol Vis Sci*. 2009;50:5159–5164.
  8. Daxer A, Fratzl P. Collagen fibril orientation in the human corneal stroma and its implication in keratoconus. *Invest Ophthalmol Vis Sci*. 1997;38:121–129.
  9. Komai Y, Ushiki T. The three-dimensional organization of collagen fibrils in the human cornea and sclera. *Invest Ophthalmol Vis Sci*. 1991;32:2244–2258.
  10. Chen L, Meng Q, Kao W, Xia Y. I $\kappa$ B kinase  $\beta$  regulates epithelium migration during corneal wound healing. *PLoS ONE*. 2011;6:e16132.
  11. Chirila TV, Hicks CR, Dalton PD, et al. Artificial cornea. *Prog Polym Sci*. 1998;23:447–473.
  12. Boote C, Dennis S, Huang Y, Quantock AJ, Meek KM. Lamellar orientation in human cornea in relation to mechanical properties. *J Struct Biol*. 2005;149:1–6.
  13. Lawrence BD, Marchant JK, Pindrus MA, Omenetto FG, Kaplan DL. Silk film biomaterials for cornea tissue engineering. *Biomaterials*. 2009;30:1299–1308.
  14. Numata K, Cebe P, Kaplan DL. Mechanism of enzymatic degradation of  $\beta$ -sheet crystals. *Biomaterials*. 2010;31:2926–2933.
  15. Lu Q, Zhang B, Li M, et al. Degradation mechanism and control of silk fibroin. *Biomacromolecules*. 2011;12:1080–1086.
  16. Jin HJ, Park J, Karageorgiou V. Water-stable silk films with reduced  $\beta$ -sheet content. *Adv Funct Mater*. 2005;15:1241–1247.
  17. Cao Y, Wang B. Biodegradation of silk biomaterials. *Int J Mol Sci*. 2009;10:1514–1524.
  18. Hu X, Shmelev K, Sun L, et al. Regulation of silk material structure by temperature-controlled water vapor annealing. *Biomacromolecules*. 2011;12:1686–1696.
  19. Kožák I, Klisenbauer D, Juhás T. UV-B induced production of MMP-2 and MMP-9 in human corneal cells. *Physiol Res*. 2003;52:229–234.
  20. Leonardi A, Cortivo R, Fregona I, Plebani M, Secchi AG, Abatangelo G. Effects of Th 2 cytokines on expression of collagen, MMP-1, and TIMP-1 in conjunctival fibroblasts. *Invest Ophthalmol Vis Sci*. 2003;44:183–189.
  21. Li DQ, Lee SB, Gunja-Smith Z, et al. Overexpression of collagenase (MMP-1) and stromelysin (MMP-3) by pterygium head fibroblasts. *Arch Ophthalmol*. 2001;119:71–80.
  22. Rockwood DN, Preda RC, Yücel T, Wang X, Lovett ML, Kaplan DL. Materials fabrication from *Bombyx mori* silk fibroin. *Nat Protoc*. 2011;6:1612–1631.
  23. Lawrence BD, Wharram S, Kluge JA, et al. Effect of hydration on silk film material properties. *Macromol Biosci*. 2010;10:393–403.
  24. Sofia S, McCarthy MB, Gronowicz G, Kaplan DL. Functionalized silk-based biomaterials for bone formation. *J Biomed Mater Res*. 2001;54:139–148.
  25. Li M, Ogiso M, Minoura N. Enzymatic degradation behavior of porous silk fibroin sheets. *Biomaterials*. 2003;24:357–365.
  26. Vepari C, Kaplan DL. Silk as a biomaterial. *Prog Polym Sci*. 2007;32:991–1007.
  27. Horan RL, Antle K, Collette A, et al. In vitro degradation of silk fibroin. *Biomaterials*. 2005;26:3385–3393.
  28. Altman GH, Diaz F, Jakuba C, et al. Silk-based biomaterials. *Biomaterials*. 2003;24:401–416.
  29. Berman M, Leary R, Gage J. Collagenase from corneal cell cultures and its modulation by phagocytosis. *Invest Ophthalmol Vis Sci*. 1979;18:588–601.
  30. Kimura K, Nomi N, Yan ZH, Orita T, Nishida T. Inhibition of poly(I:C)-induced matrix metalloproteinase expression in human corneal fibroblasts by triptolide. *Mol Vis*. 2011;17:526–532.
  31. Sengupta S, Park SH, Gil SE, et al. Quantifying osteogenic cell degradation of silk biomaterials. *Biomacromolecules*. 2010;11:3592–3599.
  32. Loesberg WA, te Riet J, van Delft FC, et al. The threshold at which substrate nanogroove dimensions may influence fibroblast alignment and adhesion. *Biomaterials*. 2007;28:3944–3951.